Organic Electronics 47 (2017) 24–34

Contents lists available at ScienceDirect

Organic Electronics

journal homepage: www.elsevier.com/locate/orgel

Optoelectronic properties of novel alkyl-substituted Triphenylamine derivatives

Jean Maria Fernandes [a, *], Chidirala Swetha [b, d], Ejjirothu Appalnaidu [b], K. Navamani [c], V. Jayathirtha Rao [b, d], M.N. Satyanarayan [a], G. Umesh [a]

[a] Optoelectronics Laboratory, Department of Physics, National Institute of Technology Karnataka, Surathkal, Mangalore 575025, India
[b] Crop Protection Chemicals Division, CSIR-Indian Institute of Chemical Technology, Uppal Road Tarnaka, Hyderabad 500007, India
[c] Theoretical Sciences Unit, Jawaharlal Nehru Centre for Advanced Scientific Research, Jakkur, Bangalore 560064, India
[d] AcSIR, CSIR-Indian Institute of Chemical Technology, Uppal Road Tarnaka, Hyderabad 500007, India

ARTICLE INFO

Article history:
Received 17 January 2017
Received in revised form
25 April 2017
Accepted 25 April 2017
Available online 27 April 2017

Keywords:
Triphenylamine (TPA)
Alkyl-substituted TPA
Hyperconjugation
Hopping transport
Carrier mobility
Impedance spectroscopy

ABSTRACT

Hole transport characteristics in three new organic compounds based on triphenylamine (TPA) moiety are presented. The effect on electrical and optical properties of TPA, attached with methyl or *tert*-butyl side groups, has been investigated through measurement of current density versus voltage (*J-V*), capacitance versus voltage (*C-V*), frequency dependent capacitance, *ac* conductivity, Impedance spectroscopy, UV-Vis spectroscopy, Photoluminescence (PL) spectroscopy and X-Ray Diffraction (XRD) studies. These measurements reveal that, the attachment of methyl or *tert*-butyl group in the *para*-position of the TPA moiety leads to improved optoelectronic properties and greater molecular stability. XRD analysis of the samples indicates that the inter-molecular distance is the lowest for TPA with *tert*-butyl side group (3.43 Å) as compared to pure TPA (3.57 Å). This leads to stronger inter-molecular interaction as evidenced by the UV-Vis spectra. PL studies indicate significant Quantum Efficiency (~30%) for alkyl attached TPA. In order to get a better understanding of the charge transport phenomena, the effect of molecular structure dynamics on charge transfer kinetics is analyzed by evaluating the charge carrier hopping rate coefficient and dynamic state factor. The dynamic state factor *b* has higher value for lower bias voltage, corresponding to dc conductivity, whereas, at higher bias, the value of *b* is smaller, indicating the dominance of *ac* conductivity. Hopping conductivity is seen to be highest for the device with *tert*-butyl substitution in TPA moiety. Our experiments indicate an order of magnitude enhancement in charge carrier mobility for alkyl-substituted TPA.

1. Introduction

Organic semiconducting materials have a wide range of potential applications in devices such as organic light-emitting diodes (OLEDs) [1–3], organic photovoltaics (OPVs) [4,5] and organic field-effect transistors (OFETs) [6,7]. Molecular engineering, leading to the synthesis of a very wide range of organic materials, together with low temperature technologies for device fabrication, have led to rapid progress in this field. Most of the organic materials employed in the electronic devices are π-conjugated materials which have delocalized electrons. It has been observed that organic materials having high Photo Luminescence (PL) efficiency exhibit rather low charge carrier mobility (~10^{-6} $cm^2V^{-1}s^{-1}$), whereas materials having large carrier mobility show much lower PL - efficiencies [8]. Triphenylamine (TPA) and its derivatives, such as α-NPD and TPD, are an important class of π-conjugated organic compounds used in OLED applications. The reported values of hole mobility for such materials fall in the range 10^{-3}-10^{-7} $cm^2V^{-1}s^{-1}$ [9,10] and the PL quantum efficiencies are seen to be about 30–40% [8]. A proper choice of the side-group for attachment to such TPA molecules is vital for achieving good device performance. In this paper, we use hole-only devices to report on the role of methyl and *tert*-butyl groups, attached to TPA molecules, on the performance of OLED devices.

The mobility in disordered organic compounds is influenced by several factors such as molecular geometry, impurities and traps. Stability of these compounds in the film form in ambient conditions can significantly affect the charge transport [11]. The stability in

* Corresponding author.
E-mail address: jean.nitk@gmail.com (J.M. Fernandes).

http://dx.doi.org/10.1016/j.orgel.2017.04.027
1566-1199/

ambient conditions depends on the HOMO-LUMO energy levels. Materials with high-lying HOMO levels are prone to oxidation, rendering them less stable [12]. However, in TPA molecules, the presence of electron deficient nitrogen and C=N double bond, lowers the HOMO energy level, leading to better stability besides enhanced hole-transport [9]. Thus, these molecules can be designed to play multifunctional roles in devices depending on their HOMO-LUMO levels, which can be suitably altered by molecular engineering.

The presence of side groups in the organic molecules leads to modifications in their electronic and optical properties. One such effect is the increase in the number of π-electrons [12]. Secondly, the presence of oxadiazole moiety reduces the steric repulsion and minimizes the torsional disorder between the neighboring units, thereby leading to a more planar structure [13]. Nagakubo et al. [14] observed a reduction in the traps at the organic-substrate interface due to the presence of *tert*-butyl groups, leading to improvement in transistor characteristics [14,15]. In this work, we show that the attachment of *tert*-butyl groups to the TPA moiety results in an order of magnitude improvement in the hole mobility (~10^{-6} $cm^2V^{-1}s^{-1}$) and thin films of this material show significant photoluminescence quantum efficiency (~30%). This is in contrast to materials having high carrier mobility [8] but low PL quantum efficiencies, typically < 1%. Further, the attachment of methyl or *tert*-butyl side group to TPA molecule increases the number of delocalized electrons and also shows higher carrier hopping rate. These investigations suggest that the alkyl-substituted TPA has good potential for OLED applications.

Attachment of *tert*-butyl group to certain organic molecules such as quarter thiophene, TTF and its derivatives, etc., improves their stability and also electronic properties due to the delocalization of π-electrons [15]. In contrast, the attachment of s-alkyl and n-alkyl side groups to these molecules does not bring in these beneficial changes. In addition, the *para*-position of the substituents is responsible for additional electron donation due to a special type of resonance contribution known as hyperconjugation [16]. It is therefore important to choose appropriate molecules as side groups for achieving the desired optoelectronic characteristics.

We present the experimental investigation of hole transport in three new compounds containing electron donating TPA moiety. The compounds denoted for further discussion as X_1, X_2 and X_3 are listed below:

a) 2-(4-(5-(4-(diphenylamino)phenyl)-1,3,4-oxadiazol-2-yl)benzylidene)malononitrile
b) 2-(4-(5-(4-(di-*p*-tolylamino)phenyl)-1,3,4-oxadiazol-2-yl)benzylidene)malononitrile
c) 2-(4-(5-(4-(bis(4-(*tert*-butyl)phenyl)amino)phenyl)-1,3,4-oxadiazol-2-yl)benzylidene) malononitrile.

In these compounds, X_2 and X_3 are obtained from compound X_1 by attaching methyl and *tert*-butyl substituents, respectively, to the TPA moiety. A brief account of their synthesis along with their NMR spectra, mass spectra, photophysical characterization and XRD has been given in the supplementary information to this paper (Scheme 1, Figs. S1–S17, Tables S1–S2). Detailed synthesis along with electrochemical and thermal properties will be reported elsewhere.

We have determined hole mobility by employing Impedance Spectroscopy which is widely used to study organic materials having dispersive transport [17]. Besides this, we have also carried out current density-voltage (*J-V*), capacitance-voltage (*C-V*) as well as frequency dependent capacitance (*C-f*) and conductivity (σ-*f*) measurements on the devices fabricated in order to get an insight into the charge transport process.

Previous theoretical studies [12,18–20] indicate that the molecular structural dynamics is responsible for interaction between the neighboring localized hopping sites. For hopping transport, electronic coupling and structural relaxation are key parameters which can be altered by appropriate side-group substitutions. Hence, we have investigated the role of side-groups on the transport and the frequency dependence of hopping rate in detail. We have also analyzed the effect of molecular structural oscillations on charge transfer kinetics in these devices.

2. Fabrication and characterization of hole-only devices

The hole-only device structure used in this study is shown in Fig. 1 (a), which includes 10 nm thick layers of *N,N′*-Di(1-naphthyl)-*N,N′*-diphenyl-(1,1′-biphenyl)-4,4′-diamine (α-NPD) on either side of compounds X_1, X_2 or X_3 to facilitate hole transport from 2,3,5,6-tetrafluoro-7,7,8,8-tetracyanoquinodimethane (F_4TCNQ) layer as well as to block electron injection from the Al cathode. The hole mobility measured in our devices is in the range 10^{-6} -10^{-7} $cm^2V^{-1}s^{-1}$ and is seen to improve with alkyl substitution. These

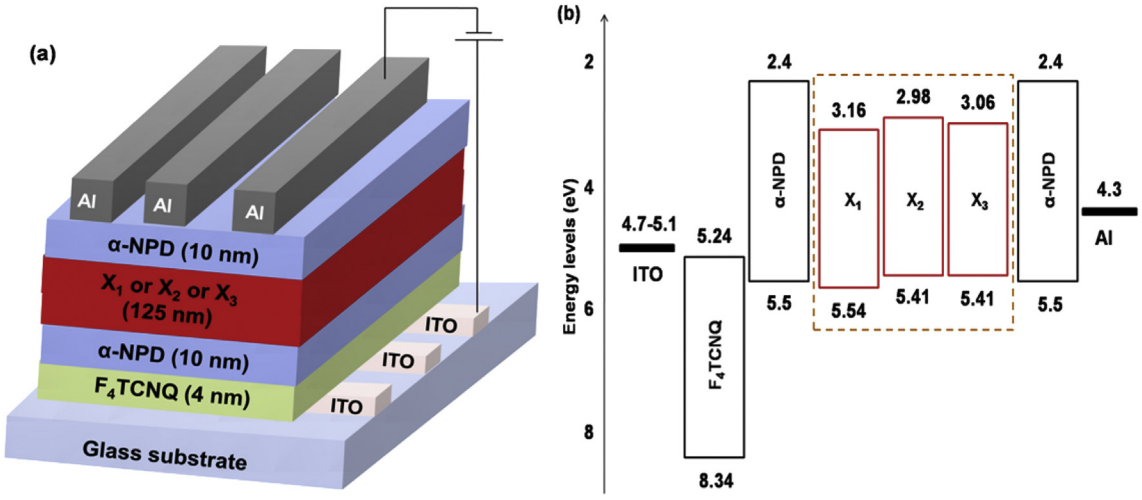

Fig. 1. **(a)** Schematic representation of the device structure and **(b)** energy level diagram of various layers, where layers X_1, X_2 and X_3 correspond to devices $\mathbf{P_1}$, $\mathbf{P_2}$ and $\mathbf{P_3}$, respectively.

materials are considered a good choice for maintaining charge carrier balance in organic electronic devices [21].

High quality F_4TCNQ (>99%) and α-NPD (>99.5%) were obtained from M/s. Lumtec, Taiwan, and were used without any further purification. Patterned indium tin oxide on glass substrate was used as the bottom anode, F_4TCNQ was used as a hole injection material, α-NPD was used as a hole transport and electron blocking material, X_1 or X_2 or X_3 was used as a hole transport material and aluminum [Al, Alfa Aesar (99.999%)] was used as cathode. The purity of the synthesized compounds was estimated by HPLC and all of them had purity better than 99%. Prior to the thin film deposition, ITO coated glass substrates (XinYan Technology Ltd., Hong Kong), with a sheet resistance of 15Ω/□, were ultrasonicated using acetone, isopropyl alcohol, DI water, in that sequence, for 15 min each and dried in flowing nitrogen to ensure that the substrate surface is free of any contaminant. This was followed by UV-Ozone treatment for 15 min which enhances the work-function of ITO. All the materials were placed in molybdenum boats, well separated from each other inside the vacuum chamber. Each boat was heated one at a time. After the deposition of the material from a particular boat, it was covered with a shutter and allowed to cool down. Then the next boat was heated to deposit the succeeding layer and the process was repeated till all the layers were deposited. Thin films of F_4TCNQ, α-NPD, X_1 or X_2 or X_3 and Al were deposited at a rate of 0.2 $Å s^{-1}$, 0.5 $Å s^{-1}$, 0.5 $Å s^{-1}$ and 5 $Å s^{-1}$, respectively, by thermal evaporation on the pre-cleaned ITO coated glass substrate under vacuum (base pressure ~ 5×10^{-6} mbar). The active area of the device was 1.6 mm^2. Fig. 1 (b) shows the HOMO and LUMO energy levels of various layers in the fabricated devices having the configuration ITO/F_4TCNQ (4 nm)/α-NPD (10 nm)/X_1 or X_2 or X_3 (125 nm)/α-NPD (10 nm)/Al. As mentioned earlier, in our devices, F_4TCNQ serves as a hole injection layer facilitating injection of holes from ITO into the adjacent hole transporting α-NPD layer. The injection of electrons from Al cathode into the device is blocked by the α-NPD layer

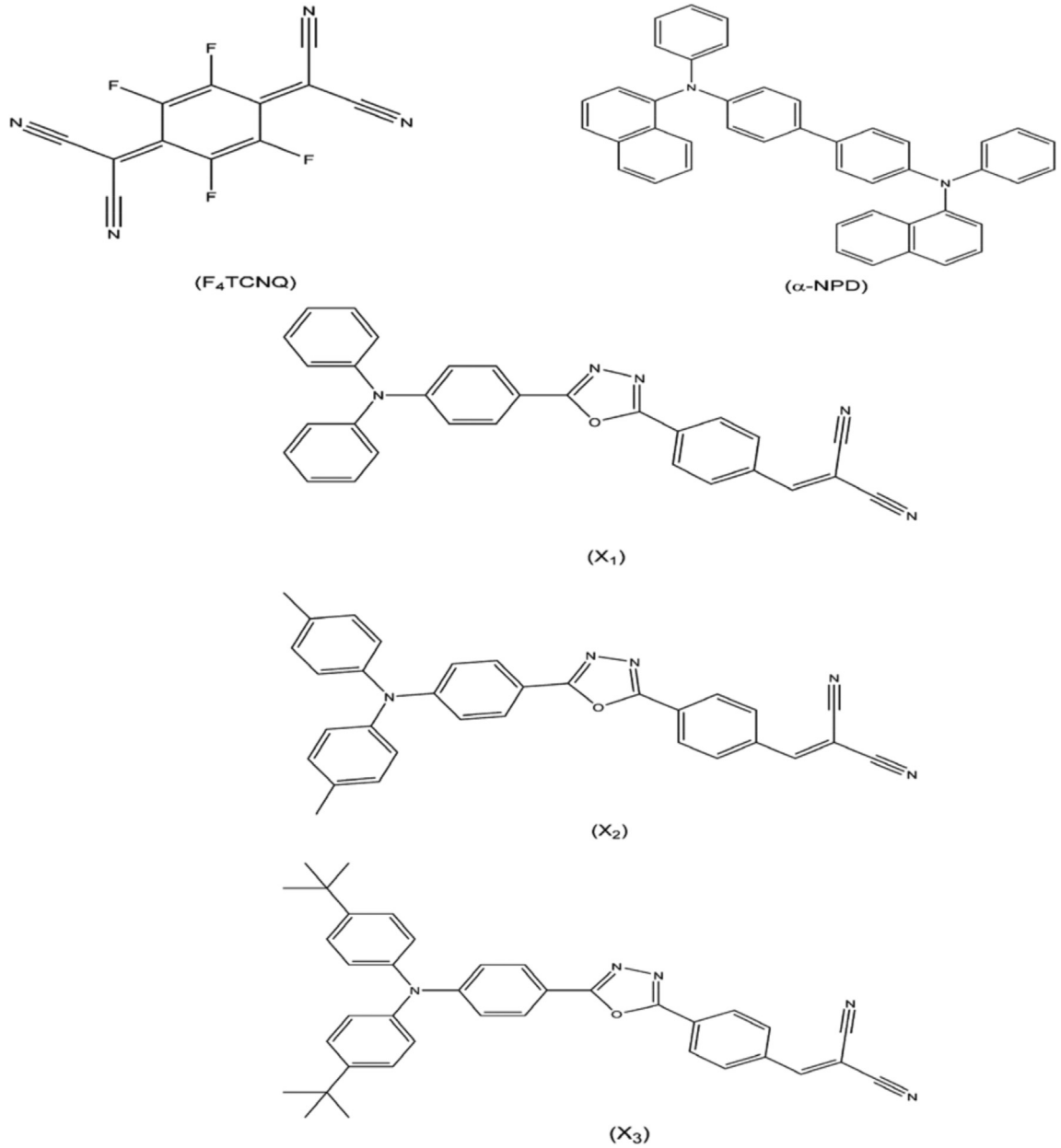

Fig. 2. Molecular structures of F_4TCNQ, α-NPD, X_1, X_2 and X_3.

adjacent to the cathode. The molecular structures of F_4TCNQ, α-NPD, X_1, X_2 and X_3 are given in Fig. 2. Methyl and *tert*-butyl functional group substituents in molecules X_2 and X_3 are expected to result in nearly planar molecular structure with highly delocalized π-electron concentration. Since the performance of organic semiconductor devices is strongly sensitive to fabrication conditions, care was taken by fabricating multiple devices, in the 3 × 3 pixel format, on a given substrate, thereby obtaining 9 identical devices for characterization. We fabricated device **P_1** using material X_1, device **P_2** using X_2 and **P_3** using X_3 as hole-only device. From the large number of devices of type **P_1**, measurements were carried out for 6 randomly chosen devices. Similar measurements were done for devices of type **P_2** and **P_3**.

Frequency dependent complex impedance, capacitance and conductivity along with voltage dependent capacitance (*C-V*) were measured at room temperature using Agilent E4980A Precision LCR Meter in the frequency range 20 Hz-1 MHz at an *ac* voltage of 100 mV. Current density-voltage (*J-V*) measurements were carried out using computer-controlled Keithley 2400 SMU. UV-Vis absorption spectra measurements were carried out using Ocean Optics Inc SD2000 spectrometer. All measurements were carried out immediately after device fabrication keeping them in open air.

3. Results and discussion

3.1. Impedance spectroscopy

Frequency dependent impedance measurements were performed to investigate the conduction mechanism in all the devices. The charge transport in organic materials is dictated by several factors, such as the quality of each of the interfaces, uniformity of the films deposited, quality of the deposited electrode films, the injected free carriers and also the polarizability of the organic molecules. In order to investigate the influence of these factors on the device operation, it is common to plot the imaginary part of the complex impedance against the real part and is termed as Cole–Cole plot. These plots, for our devices **P_1**, **P_2** and **P_3** at different dc bias voltages, are shown in Fig. 3(a–c).

The shape of the Cole-Cole plots is seen to be non-semi-circular. They may be fitted to a pair of semicircles, which individually represent the behavior of bulk and the interfaces. One may thereby extract relaxation times, corresponding respectively to the bulk and the interfaces, from each of the two semicircles [22].

The devices fabricated for our experiments are expected to behave as imperfect capacitors, owing to roughness in the interfaces and metal electrode surfaces, inhomogeneities in the film, varying film thickness and non-uniform current density distribution. For the purpose of electrochemical impedance analysis, such a device is often modeled as the circuit shown in Fig. 4 (a). In this figure, the resistance R_S corresponds to the contact resistance, R_B and R_I correspond to the bulk and interfacial resistances, respectively. The elements Q_I and Q_B, termed as 'constant phase elements (CPE)', represent the effect of inhomogeneities and surface roughness of various layers in the devices mentioned above.

The frequency dependent complex impedance of this equivalent circuit is given by the following expression [23]

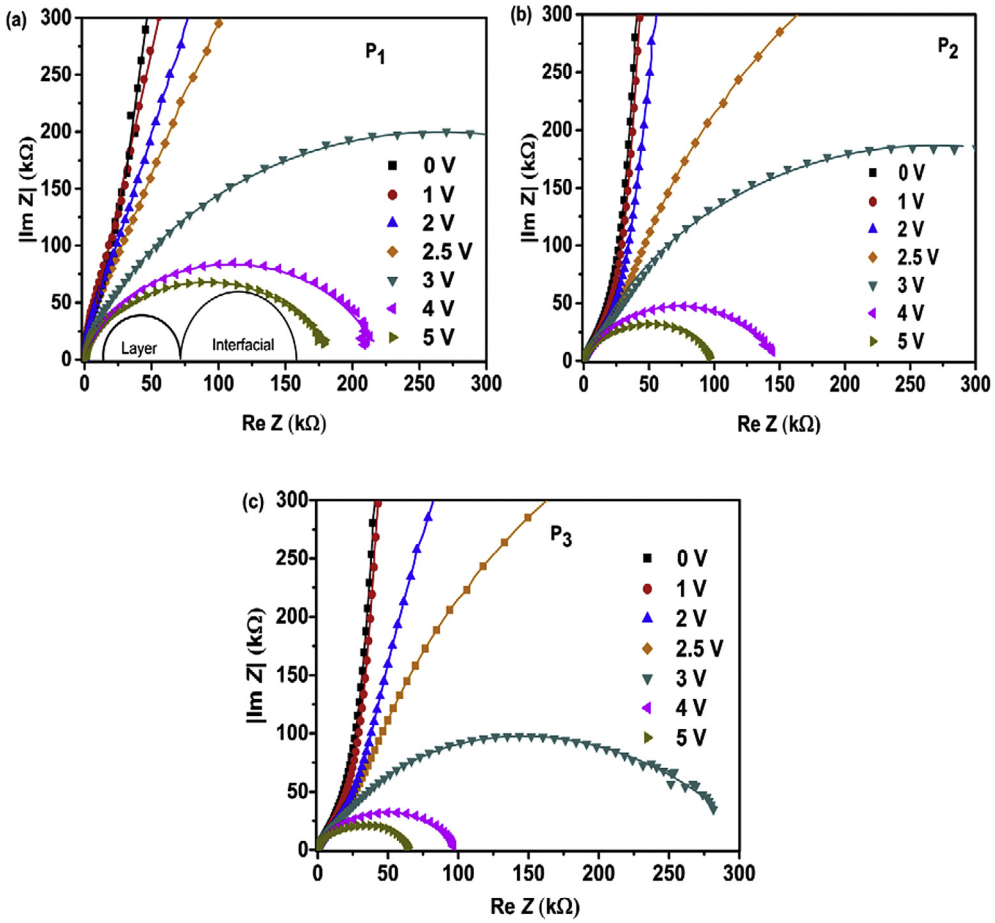

Fig. 3. Cole-Cole plots at different bias voltages for devices **(a) P_1 (b) P_2** and **(c) P_3**.

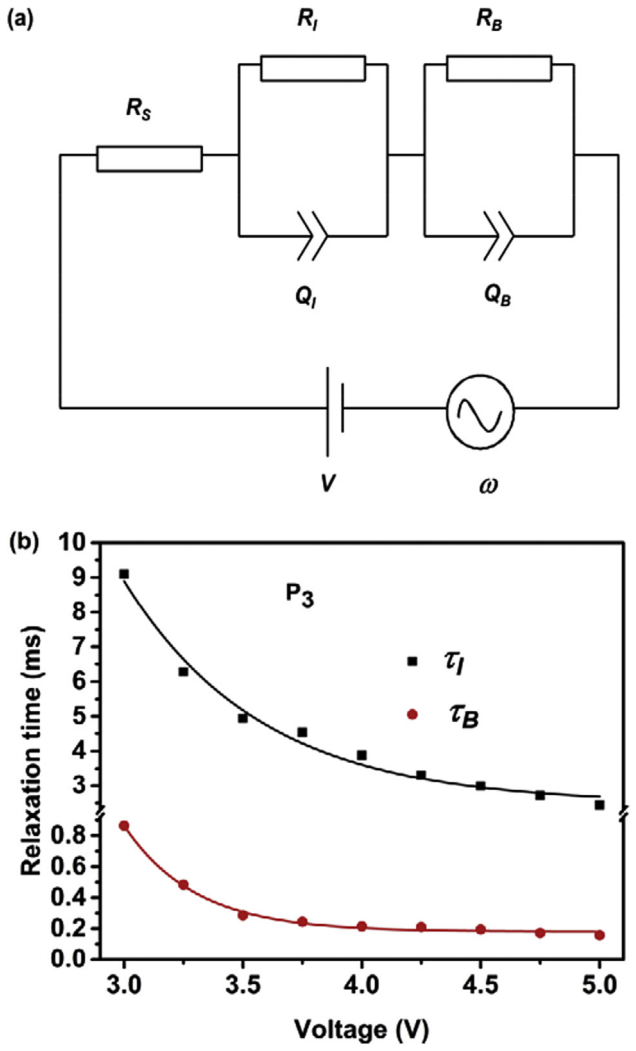

Fig. 4. **(a)** Schematic of equivalent circuit model for the analysis of Cole-Cole plot. **(b)** Relaxation times at the interface (τ_I) and bulk (τ_B) for device **P_3**.

$$Z(\omega) = R_S + \frac{R_I}{1 + (i\omega)^{n_I}\tau_I} + \frac{R_B}{1 + (i\omega)^{n_B}\tau_B} \quad (1)$$

where $\tau_I = R_I\, Q_I$ and $\tau_B = R_B\, Q_B$, with τ_I and τ_B being the average relaxation times at interface and within the organic layers.

The curves fitted using equation (1) yield values of various circuit parameters for devices **P_1**, **P_2** and **P_3** and are shown in Table 1a. From the table, it can be seen that the device **P_3** possesses lower interfacial and bulk resistance values (R_I and R_B) compared to the corresponding values for devices **P_1** and **P_2**. Therefore, the current density in **P_3** for a given bias voltage is higher than in **P_1** and **P_2**. This is also validated by the *J-V* measurements discussed later. With this in mind, we carried out a detailed investigation of device **P_3** only, which is presented in Table 1b.

From the above table, it can be seen that the values of n_I and n_B obtained for the device **P_3** lie in the range of 0.72–0.98 for different voltages. Further, the value of the series resistance (R_S) is found to be ~240 Ω which is much smaller than the values of parallel resistances (R_B and R_I). Values of Q_I and Q_B are seen to remain almost constant with applied voltage indicating space charge limited conduction mechanism [24]. The reduction in R_B and R_I with applied voltage corresponds to the reduction in the radius of the semicircles in the Cole-Cole plots as applied bias increases from 3 V to 5 V [see Fig. 3(c)] which suggests increase in the injection of charge carriers. The computed values of interfacial and bulk relaxation times ($\tau_I = R_I\, Q_I$ and $\tau_B = R_B\, Q_B$) decrease with voltage as shown in Fig. 4 (b).

It is observed that the relaxation time τ_B in bulk regime is nearly ten times less than τ_I in the interfacial regime in all the devices **P_1**, **P_2** and **P_3**, indicating the dominance of bulk transport in the devices.

3.2. Charge carrier mobility from impedance spectroscopy

The charge carrier mobility at room temperature was studied by analyzing the frequency dependence of imaginary part of the complex impedance obtained from impedance spectroscopy. Fig. 5(a–c) shows the plot of |Im(*Z*)| as a function of frequency for the devices **P_1**, **P_2** and **P_3** for a range of bias voltages.

It can be seen that in each of these plots, |Im(*Z*)| attains a peak at a particular frequency. The inverse of this frequency gives the bulk relaxation time ($\tau_B = 1/\omega$). The average carrier transit time (τ_{dc}) is related to τ_B through the relation $\tau_{dc} \approx 0.4\tau_B$ [25].

This transit time at different voltages is used to calculate the mobility as follows [26].

$$\mu(E) = \frac{d}{\tau_{dc}E} \quad (2)$$

where *d* is the thickness of the organic layer X_1 or X_2 or X_3 and *E* is the applied electric field. Theoretically, the mobility is modeled by the well-known Poole-Frenkel theory and is given by the following expression [26]

$$\mu(E) = \mu_0 \exp\left(\beta\sqrt{E}\right) \quad (3)$$

where $E = V/d$ is the applied electric field at voltage *V* and *d* is the thickness of the layer X_1 or X_2 or X_3. The plot of ln ($\mu(E)$) against $\sqrt{E}$ yields a straight line as shown in Fig. 5 (d). The slope of this line gives the Poole-Frenkel coefficient (β), and the intercept of the extrapolated graph at $E = 0$ yields the zero-field mobility (μ_0). For our devices, the value of β is seen to be in the order of ~10^{-3} $(\text{cm V}^{-1})^{1/2}$. The values of μ_0 for the devices are shown in Table 2.

We observe an order of magnitude larger hole mobility in devices **P_2** and **P_3** compared to that in **P_1** which may be ascribed to hyperconjugation resulting from the alkyl substitution on the TPA moiety. Hyperconjugation results in enhanced molecular stability due to the interaction of electrons in the σ-bond with adjacent empty or partially filled p- or π-orbital, leading to extended molecular orbitals. Methyl or *tert*-butyl groups show hyperconjugation and hence, compounds X_2 and X_3 show greater stability and also higher π-electron density compared to X_1. Unlike fluorine, methyl or *tert*-butyl groups do not possess negative inductive effects

Table 1a
Equivalent Circuit parameters for devices **P_1**, **P_2** and **P_3** at 5 V.

Device	R_I (Ω)	R_B (Ω)	Q_I (F.cm^{-2}.s$^{(n-1)}$)	Q_B (F.cm^{-2}.s$^{(n-1)}$)	n_I	n_B
P_1	1.86×10^5	24.3×10^3	1.44×10^{-8}	8.98×10^{-9}	0.95	0.76
P_2	0.94×10^5	16.5×10^3	2.72×10^{-8}	9.30×10^{-9}	0.91	0.82
P_3	0.59×10^5	16.1×10^3	4.13×10^{-8}	9.83×10^{-9}	0.98	0.81

Table 1b
Equivalent circuit parameters for device **P_3** at various voltages.

Bias (V)	R_I (Ω)	R_B (Ω)	Q_I (F.cm^{-2}.s$^{(n-1)}$)	Q_B (F.cm^{-2}.s$^{(n-1)}$)	n_I	n_B
3	2.63×10^5	88.4×10^3	3.46×10^{-8}	9.79×10^{-9}	0.75	0.72
3.25	1.8×10^5	50.1×10^3	3.47×10^{-8}	9.61×10^{-9}	0.79	0.75
3.5	1.42×10^5	31×10^3	3.48×10^{-8}	9.46×10^{-9}	0.82	0.81
3.75	1.25×10^5	25.2×10^3	3.63×10^{-8}	9.73×10^{-9}	0.87	0.83
4	0.98×10^5	23.5×10^3	3.96×10^{-8}	9.14×10^{-9}	0.92	0.83
4.25	0.83×10^5	22.5×10^3	3.97×10^{-8}	9.34×10^{-9}	0.91	0.79
4.5	0.75×10^5	21.3×10^3	3.98×10^{-8}	9.12×10^{-9}	0.95	0.80
4.75	0.68×10^5	18.1×10^3	4.01×10^{-8}	9.51×10^{-9}	0.97	0.81
5	0.59×10^5	16.1×10^3	4.13×10^{-8}	9.83×10^{-9}	0.98	0.81

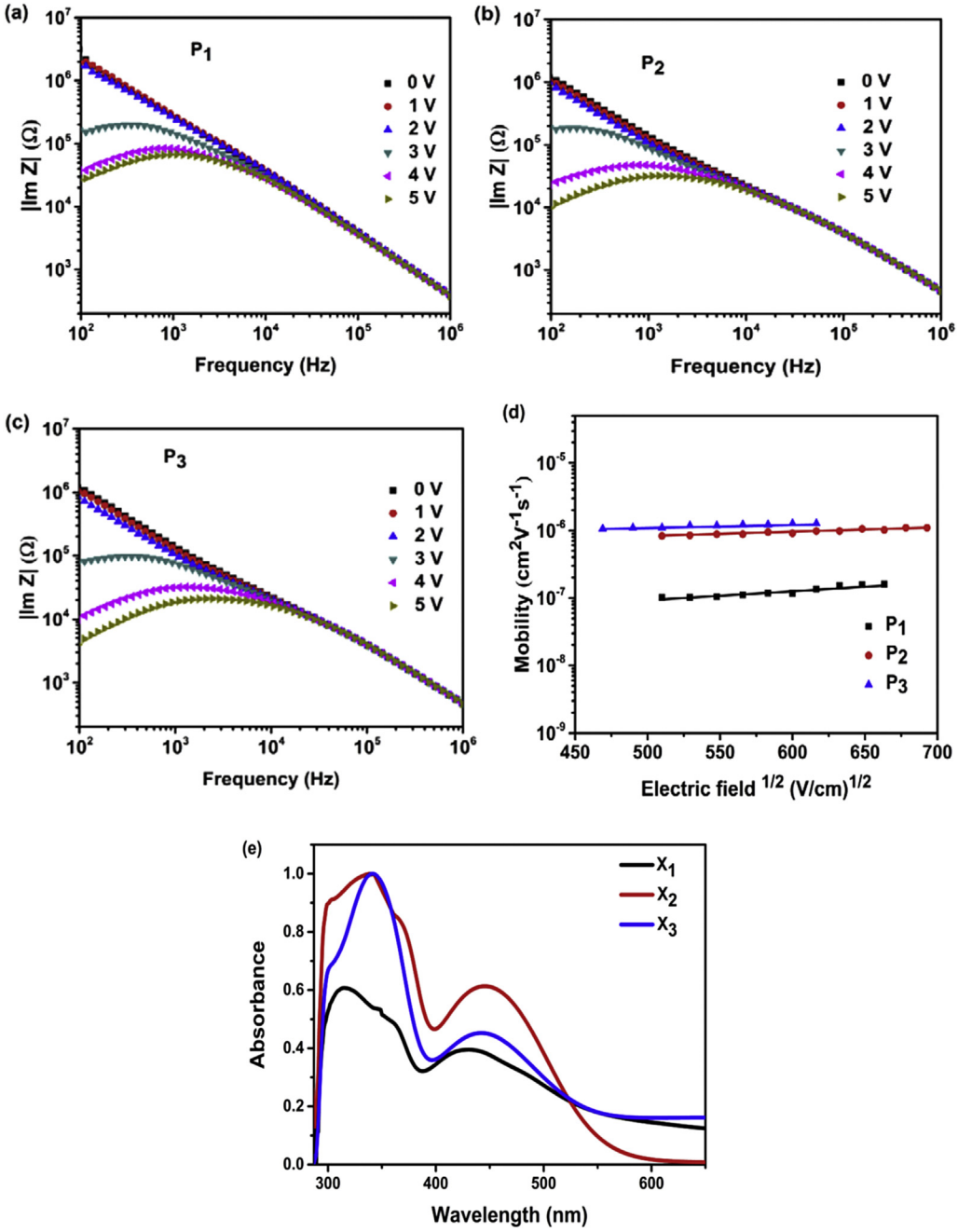

Fig. 5. Frequency dependent imaginary part of impedance of devices. **(a) P_1 (b) P_2** and **(c) P_3**. **(d)** Poole-Frenkel dependence of mobility in the devices **P_1**, **P_2** and **P_3**. **(e)** UV-Vis spectra of compounds X_1, X_2 and X_3 in thin film.

associated with electron withdrawing nature [27]. Thus, fluorine substituted compounds are typically less stable and have lower density of delocalized electrons in contrast to molecules with methyl or *tert*-butyl moieties. Further, the extended molecular orbitals ensure greater inter-molecular interaction resulting in higher charge mobility. Our experiments clearly indicate that attachment of methyl or *tert*-butyl side groups to the TPA molecules leads to an order of magnitude increase in the hole mobility as compared to a pure TPA molecule. This aspect is also corroborated by the enhanced UV-Vis absorption exhibited by devices made using X_2 or X_3 compound [Fig. 5 (e)].

3.3. J-V characteristics

The *J-V* characteristics of our devices are shown in Fig. 6(a–b).

From Fig. 6 (a), we observe higher current density and lower turn-on voltage for device **P_3** compared to devices **P_2** and **P_1** indicating improved hole injection and transport, in agreement with the impedance measurements. This is also consistent with the conclusions from mobility measurements described in section 3.2 above. With either of the two substitutions (methyl or *tert*-butyl), there is an increase in the number of delocalized π-electrons. The *para*-position of the substituent leads to highest charge distribution in the aromatic ring at that site [16]. Fig. 6 (b) shows the log *J*- log *V* plot. In this figure, the region with slope ≈2 corresponds to space-charge-limited current regime.

3.4. Charge carrier mobility from J-V characteristics

The current density in the space-charge-limited regime follows the Mott-Gurney law [28] given below

$$J = \frac{9}{8}\varepsilon_0\varepsilon_r\mu_0\frac{V^2}{d^3} \quad (4)$$

where *J* is the current density, ε_0 is the permittivity of free space, ε_r is the dielectric constant of the organic layer (X_1 or X_2 or X_3) of thickness *d*, *V* is the applied voltage and μ_0 is the zero-field charge carrier mobility. Charge carrier mobility values are extracted from the *J-V* characteristics shown in Fig. 6 (b) for devices **P_1**, **P_2** and **P_3** and are tabulated in Table 3.

The mobility values obtained from Impedance Spectroscopy and *J-V* characteristics are in good agreement with each other.

3.5. C-V measurements

Fig. 7 (a) shows capacitance normalized to geometric capacitance (C_g) plotted as a function of dc bias voltage for devices **P_1**, **P_2** and **P_3**. In our measurements, the dc bias voltage ranges from −5 V to +5 V and on this bias a 100 mV, 500 Hz *ac* signal is also imposed. This ensures that all the charge carriers and dipoles respond to the electric field and contribute to the capacitance. It is clearly seen that the capacitance equals the geometric capacitance for bias voltages < - 2 V [29]. The peak observed at higher voltages in the *C-V* plot can be attributed to the deep traps prevalent at the metal/organic and organic/organic interfaces [29]. This peak demarcates the diffusion dominated transport at lower voltages from the drift dominated transport at higher voltages. In general, there is a competition between the two transport mechanisms in the forward bias. At high forward bias, the transport across the entire device is space-charge limited [30].

Addition of *tert*-butyl group is known to reduce the trap density at the interfaces [14], which is in consonance with the shift in the peak towards lower voltage for device **P_3** as compared to **P_1** and **P_2**. Further, a smaller peak is observed at lower voltages, which is proportional to the built-in potential [31]. This peak is also seen to reduce progressively from 1.5 to 0.9 V for devices **P_1**, **P_2** and **P_3**, respectively.

3.6. C-f measurements

Since device **P_3** exhibits highest current density, we again

Table 2
Zero-field mobility obtained from Impedance Spectroscopy in devices **P_1**, **P_2** and **P_3**.

Device	Zero field mobility ($cm^{-2}V^{-1}s^{-1}$)
P_1	1.01×10^{-7}
P_2	1.06×10^{-6}
P_3	1.12×10^{-6}

Table 3
Comparison of measured mobility values in devices **P_1**, **P_2** and **P_3**.

Device	Zero field mobility ($cm^{-2}V^{-1}s^{-1}$)	
	From Impedance Spectroscopy	From *J-V* Characteristics
P_1	1.01×10^{-7}	0.98×10^{-7}
P_2	1.06×10^{-6}	1.02×10^{-6}
P_3	1.12×10^{-6}	1.07×10^{-6}

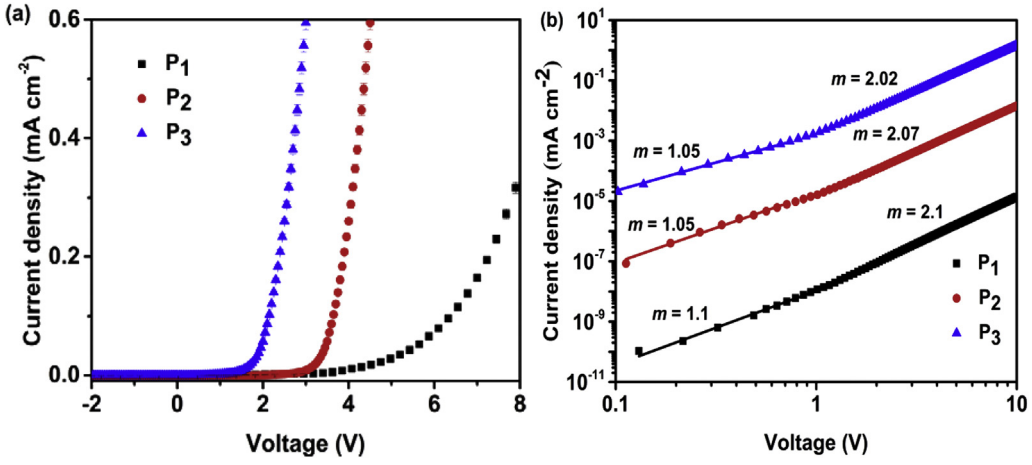

Fig. 6. **(a)** *J-V* characteristics and **(b)** log *J*- log *V* plot of devices **P_1**, **P_2** and **P_3**.

present the *C-f* measurements for only **P_3**. From the *C-f* characteristics in Fig. 7 (b), it is seen that the capacitance increases with dc bias voltage at low frequencies due to increase in dipole density and enhanced space-charge [32,33].

At higher frequencies, the molecular dipoles cannot follow the rapidly oscillating electric field, leading to reduction in capacitance to its geometric value (C_g) given by the following equation [34].

$$C_g = \frac{\varepsilon_0 \varepsilon_r A}{d} \tag{5}$$

where ε_0 is the permittivity of free space, ε_r is the dielectric constant of the organic layer (X_1 or X_2 or X_3) of thickness d and A is the area of the device. The value of this capacitance is seen to be about 0.39 nF from Fig. 7 (b). The devices **P_2** and **P_1** also have similar C_g values. The slight reduction in capacitance below C_g at very high frequencies is ascribed to the parasitic effects due to contact resistances and capacitances [35,36].

3.7. Conductivity measurements

The nature of field dependent charge transport mechanism in such devices can be ascertained from the frequency dependent conductivity (σ-f) measurements. The *ac* electrical conductivity is given by the following expression [37]

$$\sigma_{ac} = \frac{d}{A\mathrm{Re}[Z(f)]} \tag{6}$$

where d is the thickness of the organic layer (X_1 or X_2 or X_3) and A is the area of the device. As shown in Fig. 8, the *ac* conductivity for device **P_3** increases from about 10^{-9} Sm^{-1} to about 10^{-6} Sm^{-1} with voltage at low frequencies and converges to a value of the order of 10^{-5} Sm^{-1} for all voltages at higher frequencies. This clearly shows that at higher frequencies (>10 kHz) the dipole contribution to σ_{ac} becomes negligible.

The hopping transport in disordered materials is generally described by the Jonscher power law of *ac* conductivity as shown below [38].

$$\sigma_{ac} = \sigma_{dc} + B\omega^s;\ 0 < s < 1 \tag{7}$$

where σ_{dc} is the dc conductivity, ω is the frequency of the applied *ac* signal, B is a complex constant depending on the material and doping level. Further, s is determined from the slope of the curves in Fig. 8.

The values of s obtained at 5 V for devices **P_1**, **P_2** and **P_3** are seen to range from 0.430 to 0.513 and are displayed in Table 4a. Various other parameters related to hopping conduction, such as the density of localized states [$N(E_f)$] at the Fermi energy E_f, the energy W_m required by a charge carrier to move from one site to another, and the minimum hopping length R, are obtained using the following expressions [37].

$$\sigma(\omega) = \frac{\pi^3}{24} \cdot \left[N\left(E_f\right)\right]^2 \cdot \varepsilon_0 \varepsilon_r \omega R^6 \tag{8}$$

$$R = \frac{e^2}{\pi \varepsilon_0 \varepsilon_r}\left[W_m - k_B T \ln\left(\frac{1}{\omega \tau_0}\right)\right]^{-1} \tag{9}$$

$$s = 1 - \frac{6k_B T}{W_m - k_B T \ln\left(\frac{1}{\omega \tau_0}\right)} \tag{10}$$

where τ_0 is the effective relaxation time, e is the electronic charge,

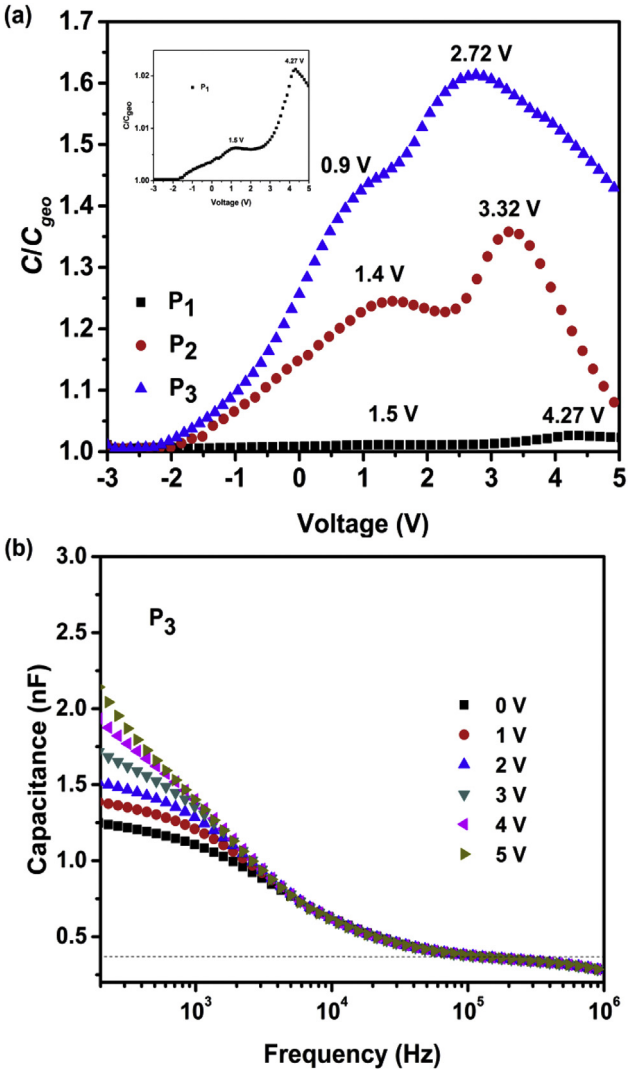

Fig. 7. **(a)** *C-V* characteristics of devices **P_1**, **P_2** and **P_3**. **(b)** Frequency dependent capacitance of device **P_3**.

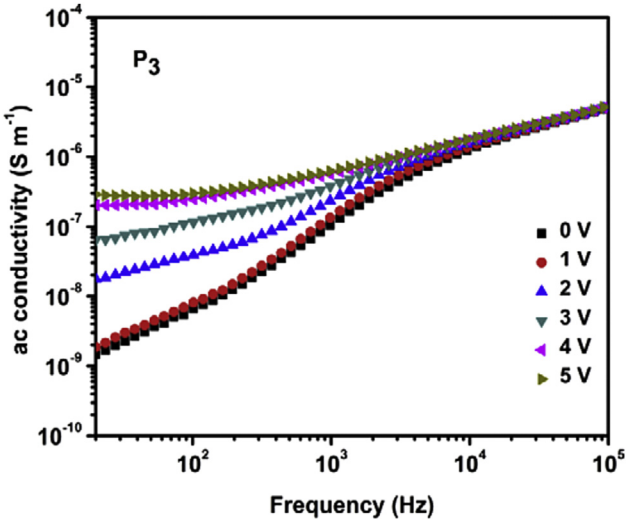

Fig. 8. Frequency dependent conductivity of device **P_3**.

Table 4a
Variation of binding energy, minimum hopping length and density of localized states for device **P_1**, **P_2** and **P_3** at 5 V.

Device	s	Hopping conductivity (σ) in 10^{-6} Sm^{-1}	W_m (eV)	R (nm)	$N(E_f)$ ($eV^{-1}m^{-3}$) at 500 Hz
P_1	0.513	8.12	0.320	5.224	5.92×10^{25}
P_2	0.451	8.54	0.284	5.887	5.48×10^{25}
P_3	0.430	19.61	0.273	6.124	4.18×10^{25}

k_B is Boltzmann's constant and T is the absolute room temperature. The values of these parameters are listed in Table 4a.

It has been shown that for hopping conduction mechanism, the value of s lies between 0 and 1 [37,39–41]. Therefore, it can be concluded that in our devices, the charge transport is dominated by hopping mechanism.

The hopping conductivity, according to density flux model can be written as [42–44].

$$\sigma(\omega) = \frac{3}{5}\varepsilon_0\varepsilon_r\frac{\partial p}{\partial t} \tag{11}$$

where ε_0 is the permittivity of free space, ε_r is the dielectric constant of the organic layer (X_1 or X_2 or X_3) and $\partial p/\partial t$ is the charge transfer rate. In our case, the average charge transfer rate between the two electrodes (ITO and Al) is calculated using equation (11).

An important objective of this investigation is to understand the role of alkyl substitution in the organic molecules such as TPA. The alkyl substitution leads to the molecular orbital overlapping between the adjacent molecular units. The size of the substituted alkyl group controls the self-assembling character as well as structural reorganization energy [12,45]. To get a clear insight on structure-property relationship, we have studied the effect of molecular structural oscillations on the electrical conductivity of our devices. Previous theoretical studies [12,18–20] confirm that the molecular structural dynamics determines the interaction between electronic and nuclear degrees of freedom, which is in turn responsible for interaction between the neighboring localized hopping sites. For hopping transport, electronic coupling and structural relaxation are key parameters which can be altered by the molecular structural disorder and appropriate side-group substitutions. Investigations over the last decade, based on Marcus theory of charge transfer rate have mostly focused on studying the effect of dynamic disorder (due to strong molecular vibrations) on charge transport in organic materials [11,18,20,43,46]. Thus, in the present study we analyze the effect of molecular structural oscillations on charge transfer kinetics for devices **P_1**, **P_2** and **P_3** through frequency dependent conductivity (Fig. 8).

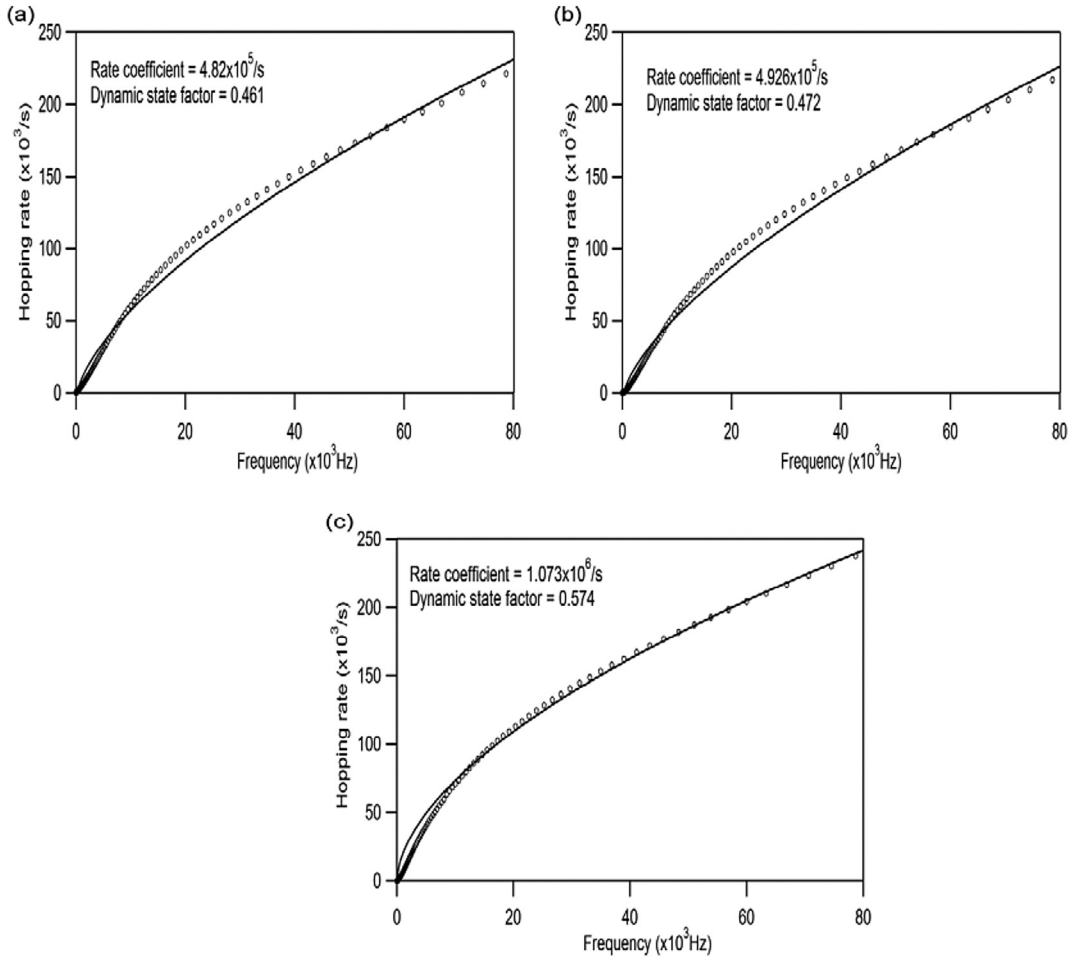

Fig. 9. The frequency dependent hopping rates for hole transport in **(a) P_1**, **(b) P_2** and **(c) P_3**.

Table 4b
Dynamic state factor (b) at different applied voltages, rate coefficient (γ) and hopping conductivity (σ) for hole transport in **P_1**, **P_2** and **P_3**.

Device	Dynamic state factor (b)						Rate coefficient (γ) in 10^5 s^{-1}	Hopping conductivity (σ) in 10^{-6} Sm^{-1}
	Applied potential (V) in volts							
	V = 0	V = 1	V = 2	V = 3	V = 4	V = 5		
P_1	0.461	0.456	0.429	0.39	0.364	0.33	4.82	8.12
P_2	0.472	0.462	0.434	0.4	0.39	0.368	4.93	8.54
P_3	0.574	0.566	0.556	0.547	0.542	0.531	10.73	19.61

The density flux model [42–44] indicates that the average hopping rate may be directly obtained from the frequency dependent conductivity for hole transport. In our experiments, the *ac* component of the applied bias significantly perturbs the nuclear motion, leading to dynamic disorder (rather than static) in agreement with the previous theoretical studies [20,44]. To analyze the dynamic disorder effect, we plot the hole hopping rate as a function of frequency [Fig. 9 (a–c)] and fit the curve to the following power law [12,18,43].

$$\frac{\partial p}{\partial t} = k(\omega) = \gamma^{1-b}(\omega)^b \tag{12}$$

where b is the fitting parameter termed 'dynamic state factor' related to the dynamic disorder. The calculated rate coefficient (γ), hopping conductivity (σ) and dynamic state factor (b) at different applied potentials for the devices **P_1**, **P_2** and **P_3** are displayed in Table 4b.

It is seen that the device **P_3** has good hole transporting ability and a hopping rate of 10.73×10^5 s^{-1} as calculated from the dynamic state factor (~0.57 at zero dc bias). This indicates significant influence of molecular oscillations on the charge transport. Of the three devices, **P_3** is seen to have the largest hopping conductivity of 19.6 μS m^{-1}, and also maximum dynamic state factor over an applied bias of 0–5 V. For this sample, the dynamic state factor is seen to decrease from 0.574 to 0.531 when the applied voltage is raised from 0 to 5 V [Table 4b]. From Fig. 8, we note that the conductivity at a dc bias of 5 V increases by a factor of 10 over a frequency range of 10 Hz–100 kHz. In contrast, at zero bias voltage, the conductivity increases by about a factor of 1000 over the same frequency range. Therefore, slope of σ-f graph is controlled by the applied potential. From Table 4b, it is noted that the dynamic state factor decreases slowly with increase in applied voltage for all the three devices, and hence we conclude that the applied potential ensures a uniform rate coefficient. It is also clear from Table 4b that the dynamic state factor b for any device generally reduces with increase in bias voltage. At smaller b, the effect of *ac* component of the bias is expected to be negligible and hence the conductivity is of the dc type. On the other hand, at zero dc bias, b is largest, indicating that the conductivity is of the *ac* type.

It is observed from Table 4a that devices **P_2** and **P_3** have lower charge carrier binding energy and density of localized states, and higher minimum hopping length at 5 V when compared to device **P_1**. This means that the charge carriers in devices **P_2** and **P_3** require lesser energy to hop between sites and they are free to move since there are fewer trap states [$N(E_f)$] where the charge carriers are localized [Table 4a]. The increase in the minimum hopping length indicates that the injected carriers can hop a greater distance at a given applied bias. However, **P_3** has much higher *ac* conductivity indicating improved carrier transport in accordance with the *J-V*, capacitance and impedance measurements.

4. Conclusion

In summary, the hole transport properties of three new compounds containing electron donating TPA moiety have been explored using impedance spectroscopy, current density-voltage (*J-V*) measurements, capacitance-voltage (*C-V*) measurements, frequency dependent capacitance (*C-f*) and frequency dependent *ac* conductivity. The alkyl substitution on the TPA moiety is shown to play an important role in the improvement of hole transport in the devices, mainly due to the increase in π electrons available for conduction on account of hyperconjugation. Various measurements show that, in particular, the presence of *tert*-butyl group in the *para*-position of the TPA moiety leads to superior device properties. The relaxation time associated with the bulk of the organic layer is found to be nearly ten times less than that at the interfaces, indicating dominance of bulk charge transport in all the devices. The value of bulk hole mobility determined in the device is observed to increase by an order of magnitude with alkyl substitution on the TPA moiety in these compounds. Different parameters such as hopping length, binding energy, extended molecular orbitals and the effective localized density of states are determined to understand the charge transport mechanism and relate it to the device performance. The experimental results show that the structural oscillations due to a small applied *ac* electric field influence the charge transport mechanism and are in agreement with the previous theoretical studies. The frequency dependence on hopping rate is analyzed by the dynamic state factor which determines the crossover mechanism between *ac* and dc conductivity. The electrical and optical properties of these compounds indicate that they can be potential candidates for applications such as OLEDs.

Acknowledgements

Among the authors, JMF acknowledges National Institute of Technology Karnataka, Surathkal, for granting research fellowship and VJR thanks TAPSUN-NWP0055 grant of CSIR, New Delhi, India. The authors gratefully acknowledge useful discussions with Dr. Kartick Tarafder on theoretical analysis presented in this work. This work was financially supported by the Ministry of Electronics and Information Technology, Government of India 12(3)/2010-PDD, through a research grant.

Appendix A. Supplementary data

Supplementary data related to this article can be found at http://dx.doi.org/10.1016/j.orgel.2017.04.027.

References

[1] C.W. Tang, S.A. Vanslyke, Organic electroluminescent diodes, Appl. Phys. Lett. 51 (1987) 913–915.
[2] E. Gondek, S. Całus, A. Danel, A.V. Kityk, Photoluminescence and electroluminescence of methoxy and carboethoxy derivatives of 1,3-diphenyl-1H-pyrazolo[3,4-b]quinoline, Spectrochim. Acta Part A Mol. Biomol. Spectrosc. 69 (1) (2008) 22–26.
[3] Godumala Mallesham, Chidirala Swetha, Surukonti Niveditha, Maneesha Esther Mohanty, Nanubolu Jagadeesh Babu, Arunandan Kumar, Kotamarthi Bhanuprakash, Vaidya Jayathirtha Rao, Phosphine oxide functionalized pyrenes as efficient blue light emitting multifunctional materials for

organic light emitting diodes, J. Mater. Chem. C 3 (6) (2015) 1208–1224.
[4] W. Cao, J. Xue, Recent progress in organic photovoltaics: device architecture and optical design, Energy Environ. Sci. 7 (2014) 2123–2144.
[5] Luyao Lu, Mary Allison Kelly, Wei You, Luping Yu, Status and prospects for ternary organic photovoltaics, Nat. Photonics 9 (8) (2015) 491–500.
[6] Kyohei Nakano, Hiroaki Iino, Takayuki Usui, Jun-ichi Hanna, Bulk mobility of polycrystalline thin films of quaterthiophene derivatives, Appl. Phys. Lett. 98 (10) (2011) 103302.
[7] Y. Chen, B. Lee, H.T. Yi, S.S. Lee, M.M. Payne, S. Pola, C.-H. Kuo, Y.-L. Loo, J.E. Anthony, Y.—T. Tao, V. Podzorov, Dynamic character of charge transport parameters in disordered organic semiconductor field-effect transistors, Phys. Chem. Chem. Phys. 14 (2012) 14142–14151.
[8] J. Liu, H. Zhang, H. Dong, L. Meng, L. Jiang, L. Jiang, Y. Wang, J. Yu, Y. Sun, W. Hu, A.J. Heeger, High mobility emissive organic semiconductor, Nat. Commun. 6 (10032) (2015) 1–8.
[9] Shu K. So, Shing C. Tse, Ka L. Tong, Charge transport and injection to phenylamine-based hole transporters for OLEDs applications, J. Disp. Technol. 3 (2) (2007) 225–232.
[10] J.M. Fernandes, M.R. Kiran, H. Ulla, M.N. Satyanarayan, G. Umesh, Investigation of hole transport in α-NPD using impedance spectroscopy techniques with F_4TCNQ as hole-injection layer, Superlattices Microstruct. 83 (2015) 766–775.
[11] A.A. Kocherzhenko, Charge Transport in Disordered Molecular Sytems, Ph.D. Dissertation, Delft University Press, The Netherlands, 2011.
[12] K. Navamani, G. Saranya, P. Kolandaivel, K. Senthilkumar, Effect of structural fluctuations on charge carrier mobility in thiophene, thiazole and thiazolothiazole based oligomers, Phys. Chem. Chem. Phys. PCCP 15 (41) (2013) 17947–17961.
[13] Ayan Datta, Swapan K. Pati, Charge-transfer induced large nonlinear optical properties of small Al Clusters: Al4M4(M = Li, Na, and K), J. Phys. Chem. A 108 (44) (2004) 9527–9530.
[14] J. Nagakubo, M. Ashizawa, T. Kawamoto, A. Tanioka, T. Mori, Stabilization of organic field-effect transistors by tert-butyl groups in dibenzotetrathiafulvalene derivatives, Phys. Chem. Chem. Phys. PCCP 13 (32) (2011) 14370–14377.
[15] T. Higashino, Y. Akiyama, H. Kojima, T. Kawamoto, T. Mori, Organic semiconductors and conductors with *tert*-butyl substituents, Crystals 2 (2012) 1222–1238.
[16] Addy Pross, Leo Radom, Noel V. Riggs, A theoretical approach to substituent effects. Structural consequences of methyl hyperconjugation. Methyl tilt angles and carbon-hydrogen bond lengths, J. Am. Chem. Soc. 102 (7) (1980) 2253–2259.
[17] E. Barsoukov, J.R. Macdonald, Impedance Spectroscopy Theory, Experiment, and Applications, Wiley, USA, 2005.
[18] Yuri A. Berlin, Ferdinand C. Grozema, Laurens D.A. Siebbeles, Mark A. Ratner, Charge transfer in donor-bridge-acceptor systems: static disorder, dynamic fluctuations, and complex kinetics, J. Phys. Chem. C 112 (29) (2008) 10988–11000.
[19] A. Troisi, D.L. Cheung, Transition from dynamic to static disorder in one-dimensional organic semiconductors, J. Chem. Phys. 131 (1) (2009) 014703.
[20] A. Troisi, Charge transport in high mobility molecular semiconductors: classical models and new theories, Chem. Soc. Rev. 40 (5) (2011) 2347–2358.
[21] Louis M. Leung, Yik-Chung Law, Michael Y. Wong, Tik-Ho Lee, Kin Ming Lai, Lok-Yee Tang, Charge balance materials for homojunction and heterojunction OLED applications, Front. Optoelectron. China 2 (4) (2009) 435–441.
[22] J. Liu, C.-G. Duan, W.-G. Yin, W.-N. Mei, R.W. Smith, J.R. Hardy, Large dielectric constant and Maxwell-Wagner relaxation in Bi2/3Cu3Ti4O12, Phys. Rev. B 70 (2004) 144106.
[23] J.-P. Diard, B. Le Gorrec, C. Montella, Handbook of Electrochemical Impedance Spectroscopy-electrical Circuits Containing CPEs, Bio-logic Science Instruments, 2013.
[24] S.H. Kim, S.C. Lim, J.H. Lee, T. Zhyung, Conduction mechanism of organic semiconductor AlQ3: impedance spectroscopy analysis, Curr. Appl. Phys. 5 (2005) 35–37.
[25] Durgesh C. Tripathi, Awnish K. Tripathi, Y.N. Mohapatra, Mobility determination using frequency dependence of imaginary part of impedance (Im Z) for organic and polymeric thin films, Appl. Phys. Lett. 98 (3) (2011) 033304.
[26] S.W. Tsang, S.K. So, J.B. Xu, Application of admittance spectroscopy to evaluate carrier mobility in organic charge transport materials, J. Appl. Phys. 99 (1) (2006) 013706.
[27] Kai Lin Woon, Zakaria Nurul Nadiah, Zainal Abidin Hasan, Azhar Ariffin, Show-An Chen, Tuning the singlet-triplet energy splitting by fluorination at 3,6 positions of the 1,4-biscarbazoylbenzene, Dyes Pigments 132 (2016) 1–6.
[28] M.A. Lampert, P. Mark, Current Injection in Solids, New York, Academic Press, 1970.
[29] Akanksha Sharma, Pramod Kumar, Budhi Singh, Sumita Ray Chaudhuri, Subhasis Ghosh, Capacitance-voltage characteristics of organic Schottky diode with and without deep traps, Appl. Phys. Lett. 99 (2) (2011) 023301.
[30] Durgesh C. Tripathi, Y.N. Mohapatra, Charge transport across organic heterostructure: role of interfacial density of states, J. Appl. Phys. 116 (6) (2014) 064509.
[31] Akanksha Sharma, Sarita Yadav, Pramod Kumar, Sumita Ray Chaudhuri, Subhasis Ghosh, Defect states and their energetic position and distribution in organic molecular semiconductors, Appl. Phys. Lett. 102 (14) (2013) 143301.
[32] J.M. Fernandes, M.R. Kiran, H. Ulla, M.N. Satyanarayan, G. Umesh, Investigation of hole-injection in a-NPD using capacitance and impedance spectroscopy techniques with F_4TCNQ as hole-injection layer: initial studies, Superlattices Microstruct. 76 (2014) 385–393.
[33] S. Nowy, W. Ren, J. Wagner, J.A. Weber, W. Brutting, Impedance spectroscopy of organic hetero-layer OLEDs as a probe for charge carrier injection and device degradation, Proc. SPIE 7415 (2009), 74150G-74150G-12.
[34] Stefan Nowy, Wei Ren, Andreas Elschner, Wilfried Lövenich, Wolfgang Brütting, Impedance spectroscopy as a probe for the degradation of organic light-emitting diodes, J. Appl. Phys. 107 (5) (2010) 054501.
[35] Y.F. Xu, Y.S. Tao, H.J. Zhang, X.Z. Chen, G.H. Cao, Z.A. Xu, H.Y. Li, S.N. Bao, P. He, Impedance spectroscopy study on transport properties of N,N′-diphenyl-N,N′-bis(1-naphthyl)-1,1′-biphenyl-4,4′-diamine, Phys. B Condens. Mat. 362 (1–4) (2005) 35–40.
[36] W. Brutting, H. Riel, T. Beierlein, W. Riess, Influence of trapped and interfacial charges in organic multilayer light-emitting devices, J. Appl. Phys. 89 (2001) 1704–1712.
[37] C.K. Suman, Jinyoung Yun, Seohee Kim, Sin-Doo Lee, Changhee Lee, AC impedance spectroscopic studies of transport properties in metal oxide doped α-NPD, Curr. Appl. Phys. 9 (5) (2009) 978–984.
[38] A.K. Jonscher, The 'universal' dielectric response, Nature 267 (5613) (1977) 673–679.
[39] S.R. Elliott, A theory of a.c. conduction in chalcogenide glasses, Philos. Mag. 36 (6) (1977) 1291–1304.
[40] R.M. Hill, A.K. Jonscher, DC and AC conductivity in hopping electronic systems, J. Non-Cryst. Solids 32 (1–3) (1979) 53–69.
[41] S. Ouled Mansour, B. Louati, K. Guidara, AC conductivity and dielectric behavior of high-temperature form of copper silver phosphate, Ionics 21 (7) (2015) 1973–1982.
[42] K. Navamani, K. Senthilkumar, Forth—back oscillated charge carrier motion in dynamically disordered hexathienocoronene molecules: a theoretical study, Phys. Chem. Chem. Phys. 17 (27) (2015) 17729–17738.
[43] K. Navamani, K. Senthilkumar, Effect of structural fluctuations on charge carrier dynamics in triazene based octupolar molecules, J. Phys. Chem. C 118 (48) (2014) 27754–27762.
[44] K. Navamani, K. Senthilkumar, Effect of dynamic disorder on charge carrier dynamics in Ph4DP and Ph4DTP molecules, RSC Adv. 5 (48) (2015) 38722–38732.
[45] P.N. Prasad, Frontiers of Polymers and Advanced Materials, Springer, 2012.
[46] R.P. Fornari, A. Troisi, Theory of charge hopping along a disordered polymer chain, Phys. Chem. Chem. Phys. PCCP 16 (21) (2014) 9997–10007.